Sampling considerations when analyzing micrometric-sized particles in a liquid jet using laser induced breakdown spectroscopy

Authors: C. B. Faye [a], T. Amodeo [a], E. Fréjafon [a], N. Delepine-Gilon [b] and C. Dutouquet [a,*]

[a] Institut National de l'Environnement Industriel et des Risques (INERIS/DRC/CARA/NOVA), Parc Technologique Alata, BP 2, 60550 Verneuil-En-Halatte, France

[b] Institut des Sciences Analytiques, 5 rue de la Doua, 69100 Villeurbanne, France

*Corresponding author: Christophe Dutouquet

christophe.dutouquet@ineris.fr

Tel.: +33 3 44 61 81 46

Fax: +33 3 44 55 68 72

Abstract

Pollution of water is a matter of concern all over the earth. Particles are known to play an important role in the transportation of pollutants in this medium. In addition, the emergence of new materials such as NOAA (Nano Objects, their Aggregates and their Agglomerates) emphasize the need to develop adapted instruments for their detection. Surveillance of pollutants in particulate form in waste waters in industries involved in nanoparticle manufacturing and processing is a telling example of possible applications of such instrumental development. The LIBS (Laser-Induced Breakdown Spectroscopy) technique coupled with the liquid jet as sampling mode for suspensions was deemed as a potential candidate for on-line and real time monitoring.

With the final aim in view to obtain the best detection limits, the interaction of nanosecond laser pulses with the liquid jet was examined. The evolution of the volume sampled by laser pulses was estimated as a function of the laser energy applying conditional analysis when analyzing a suspension of micrometric-sized particles of borosilicate glass. An estimation of the sampled depth was made. Along with the estimation of the sampled volume, the evolution of the SNR (Signal to Noise Ratio) as a function of the laser energy was investigated as well. Eventually, the laser energy and the corresponding fluence optimizing both the sampling volume and the SNR were determined. The obtained results highlight intrinsic limitations of the liquid jet sampling mode when using 532 nm nanosecond laser pulses with suspensions.

Keywords: suspensions of micrometric-sized particles, LIBS, liquid jet, NOAA (Nano Objects, their aggregates and their agglomerates)

1. Introduction

Pollution of air and water are major concerns all over the world. At European union level, the importance of the issue of water pollution is stressed by the adoption of a framework directive aiming at achieving a good ecological and chemical status of waters by 2015. Though the water framework directive does not specifically target particles, these are known to play a major role in pollutant transportation. Furthermore, the issue of particle release in liquids could become even more compelling with the advent of new objects such as NOAA (Nano Objects, their Agglomerates and Aggregates). Surveillance of pollutants in particulate form possibly released in waste waters by industries involved in nanoparticle manufacturing and processing is a telling example of applications requiring instrumental developments. The above considerations emphasize the need to develop a technique adapted to particle detection allowing in-situ and real-time elemental identification and mass concentration determination of particles suspended in liquids. The LIBS (Laser-Induced Breakdown Spectroscopy) technique was deemed as a potential candidate to tackle such issue [1-2].

LIBS consists in focusing a powerful laser pulse on a material (solid, liquid, gas, aerosol, nanoparticle suspensions) whose elemental composition is to be determined. The strong heating of the sample at the focusing spot leads to the ignition of a hot and luminous transient ionized gas called plasma. Plasma light contains the signature of all the chemical elements the interrogated material is made of. This signature is read by sending the emitted light through a spectrometer equipped with a detector. The LIBS signal presents itself as an optical emission spectroscopy spectrum displaying lines corresponding to the detected elements. The features of LIBS (all optical technique, fast, non intrusive, no sample preparation, remote and stand-off analysis possible) do make it a promising analytical chemistry technique intended to be operated at industrial or environmental sites. Current elemental analysis techniques require time consuming procedures involving several steps such as on-site sampling, preparation back to the laboratory prior to the analysis itself.

LIBS has already been applied to particle detection in liquids either for environmental or industrial purposes [3-10]. Different sampling modes such as cuvette [4,6,7,8,9,10], liquid jet [3,5,6] and deposition on filters (following ultrafiltration) [6] were coupled with nanosecond duration laser pulses at 532 nm (for most of them) testing various energies, focusing and collection paths. The analyses were carried out on particles of various chemical natures with sizes ranging from a few hundreds of nanometers to a few tens of micrometers. Detection limits were found on average of about a few tens to a few hundreds of micrograms per liters. Continuous monitoring of liquid samples like that needed in the above mentioned possible application is facilitated using the liquid jet configuration. Two recent papers have shed light on peculiarities encountered

when dealing with particle detection using the liquid jet. Snyder et al.[11] have emphasized the need for a careful data processing and rejection of spectra free of signal where no particles are sampled, thereby highlighting the difference between a supposed homogeneous solution and a suspension of particles with their discrete nature. The upper size limit of complete vaporization was investigated by Diaz Rosado et al. [12] demonstrating incomplete vaporization of micrometric-sized alumina particles above a diameter of around 800 nm.

In this paper, the attention was focused on the volume sampled by the laser pulses and on the SNR (Signal to Noise Ratio) of the LIBS signal. Both sampling volume and SNR evolutions were examined as a function of the laser energy. The obtained sampling volume was compared to the maximum accessible volume calculated considering the liquid jet thickness times the estimated laser beam diameter right where laser pulses strike the liquid jet. A "sampled depth" representing the layer thickness within which the analyte is vaporized thereby contributing to the LIBS signal was estimated. Eventually, a laser energy and an estimation of the corresponding fluence were found that maximize both the sampling volume and the SNR, thereby designating the optimal laser energy / fluence when irradiating a suspension with laser pulses of 5 ns duration at 532 nm. The limitations inherent to the coupling of the liquid jet with the LIBS technique when analyzing micrometric-sized particles are presented and discussed.

2. Experimental set-up

2.1 The liquid sampling mode

The liquid jet sampling mode (designed by IVEA solution French supplier of LIBS systems) has been retained for the experiments on the detection of particles in liquids. The suspension is flowed through a flexible tube connected to a capillary using a peristaltic pump. It is then ejected from the capillary in the form of a stable liquid jet with a 1 mm thickness at a flow rate of 150 mL min^{-1}. Laser pulses were focused on the jet around 10 mm downstream its output. The IVEA system also includes air sweeping in front of the focusing lens to avoid droplet deposition caused by splashing. Micrometric displacements of the liquid jet was assured using two linear translation stages allowing its precise positioning with respect to the focused laser pulses.

2.2 LIBS experimental set-up

The LIBS experimental set-up is presented on figure 1. Laser pulses with energies varying from 3 to 60 mJ and durations of 4 ns fired by a 532 nm Q-switched laser (Quantel Brilliant) operating at 20 Hz were first spatially expanded to three times the initial beam diameter (6 mm). They were then directed through a half wave

plate and a Glan polarizer for energy attenuation. A dichroïc mirror fully reflective at 532 nm but otherwise transparent directed the beam toward a 100 mm focal length lens allowing focusing laser pulses on the liquid jet. The mirror was positioned so as to make a 90 degree angle between the optical axis of the beam expander and that of the focusing lens. Such optical path makes light collection along the focusing axis possible, given that the dichroïc mirror is transparent to almost all wavelengths but that of the laser. The LIBS signal was collected along the focusing axis through the 100 mm focal length lens and focused on the entrance of a 1 mm core diameter optical fiber (Ocean Optics) using a 35 mm focal lens. Optical emission spectra were retrieved from a spectrometer (Horiba Jobin Yvon, model iHR320) equipped with a gated intensified CCD camera (Andor iStar model DH734-18F-03). Time resolved measurements are made possible with such detector by triggering signal recording when the laser pulses are fired and recording over the required duration by selecting the appropriate integration time (with accessible time resolution of around 2 ns). Another iCCD camera (same model as above) equipped with UV lens objective (Nikon model 78 mm F/3.8) was positioned on the axis perpendicular to that of laser focusing to allow monitoring the position of the liquid jet. The focal spot size had to be estimated to evaluate the laser fluence. The estimation was made assuming a perfect Gaussian beam profile and considering the beam section at $1/e^2$ of the maximum pulse intensity using marks drilled in a copper plate for different energies as explained in section (4.3). Crater diameters were measured using a Zeiss microscope (Axio Imager M1m).

3. Foreword

3.1 Particle features

Duke scientific (dry glass NIST traceable size standards, 9000 Series Borosilicate Glass) certified particle size standards with lots of particles with nominal diameters of 2, 5, 8 and 10 µm were used in this work. Four test suspensions containing particles with the aforementioned characteristics and concentrations of around 10^{-4} g / cm^3 were prepared using ultrapure water (Millipore water purification system Milli-Q Advantage A10) without surfactant. Particle morphology, elemental composition and sizes were controlled using SEM (Scanning Electron Microscopy, FEI Company, model Quanta 400) analysis. Size distributions of the suspensions were obtained using LDS (Laser Diffraction Spectrometry, Malvern Instruments model Mastersizer 2000). It should be noted that these measurements were performed while continuously agitating the suspensions with a magnetic stirrer, the latter being utilized in the course of the LIBS experiments. SEM images of 5µm sized particles are presented on figure 2. Their nominal diameter was found of around 5 ± 0.5 µm with a spherical shape. Their

elemental chemical composition was analyzed through EDX (Energy Dispersive X-ray) showing that Si, Ca and Al are elements found with the largest abundance. Size distributions of the four lots are displayed on figure 3. Particle features were eventually found in good agreement with the data sheets provided by the manufacturer even after having been stirred.

3.2 Calculation of the sampling volume

As emphasized by Hahn et al. [13] in previous work, the analysis of particles using the LIBS technique requires adapted data processing. Either suspended in the air or in a liquid, particles have a discrete nature. This means that not all the laser shots lead to particle detection. Under these conditions, the usual ensemble-averaging technique aiming at improving the signal-to-noise ratio by systematically adding the signal originating from several laser shots in one final single spectrum is no longer adapted. An alternative method named conditional analysis was proposed by Carranza and Hahn [14-15] in order to improve LIBS signal to noise ratio when dealing with particle detection. It consists in recording individual spectra, each of them corresponding to one unique laser shot. The ratio of the number of spectra having sampled one particle (spectra therefore considered as positive) to that of the total amount of laser shots fired [16] yields the PSR (or Particle Sampling Rate). Spectra free of signal are discarded prior to the addition leading to the final spectrum. The latter is obtained by adding the intensities of all the positive spectra and multiplying the resulting sum by the particle sampling rate (PSR). It was shown by Panne and Hahn [17] that the sampling volume could be estimated from the particle sampling rate provided that the latter was not higher than a value of around 10 %. With this condition fulfilled, an estimation of the sampling volume can be inferred from equation 1 below:

$$V_S = \frac{PSR}{100 \times C} \qquad \text{Equation 1}$$

with V_S the sampling volume, C the number concentration of particles and PSR the particle sampling rate. This approach was applied in order to assess the volume of liquid sampled when analyzing particles using LIBS.

4. Results and discussion

4.1 Line selection and temporal settings

Given the relative abundances of the various elements constituting borosilicate glass particles (see section 3.1) and the efficiency of the detection system as a function of wavelength, the Ca I line at 422.672 nm (A_{ki} = 21.8 × 10^7 s^{-1}, E_i (eV) = 0.0 and E_k (eV) 2.9325118) was selected for these experiments. The evolution of

the sampling volume and that of the SNR were estimated through the LIBS signal as a function of laser energy. Accordingly, time delays and gate widths were adjusted after having analyzed LIBS temporal evolution recorded when irradiating a $CaSO_4$ solution for each laser energy. Such procedure was motivated bearing in mind that the plasma volume tends to enlarge when increasing the energy. Such enlargement results in a much slower cooling speed thereby temporally shifting the time delays at which the recording of the given line of an element is optimized [18,19]. The obtained results are presented on figure 4. The optimized time delays were indeed found slightly shifted from one laser energy to another with values of 0.25, 1, 1, 2, 3, 4, 5, 5 µs for laser energies corresponding to 3, 5, 7, 10, 15, 30, 45, 60 mJ. The gate width was fixed to 5 µs.

4.2 PSR calculation

The determination of the PSR prior to that of the sampling volume necessitates appropriate data processing. A two step filtering procedure was utilized as suggested by Asgill and Hahn [20]. A first filtering algorithm was designed to select positive spectra. It was operated using a criterion designating a spectrum as positive when the peak of the line of interest minus its background was found higher than a threshold value defined as n times the noise intensity. The latter is calculated on both sides of the line (in its vicinity) of interest using the standard deviation formula. Several values of n were tested when running the algorithm for a given series of spectra. The selection of the threshold level implying the fixing of the n number was set using the following approach. Obviously, low values of n lead to select spectra that do not correspond to real lines. The algorithm is very likely to be misled if the accumulation of noise on pixels where the line of interest is expected to emerge happens to be higher than the defined threshold value. This eventually results in the recording of the so called false positives. Contrariwise, some of the real positives may be accidentally discarded when choosing high values for n. Thus, the n values were chosen so as to minimize the amount of false positives found when visually inspecting the retained spectra.

A second filtering algorithm was implemented to refine the selection. Indeed, poor repeatability of PSR calculation was obtained when only applying the above defined criterion. In addition, lots of the selected spectra (though not clearly identified as false positives) happen to display a very low signal to background ratio. They made the PSR increase without contributing much to the final signal. Thus, the intensity of the Ca line normalized to the maximum recorded intensity was plotted as a function of the percentage of spectra marked as positives (figure 5). Eventually, the PSR repeatability was found to stabilize when suppressing 30% of the

spectra marked as positives whose intensities were below 10% of the highest recorded intensity. This is tantamount to neglecting minor hits corresponding to partial ablation of the particles. The PSR is therefore slightly underestimated by not taking into account minor hits.

4.3 Evolution of the sampling volume as a function of laser energy

A first series of experiments was carried out with the aim in view to investigate the evolution of the sampling volume as a function of laser energy. Three series of spectra of 1000 laser shots each were recorded for several energies ranging from 3 to 60 mJ. Sampling volume variations as a function of laser energy is presented on figure 6. The particle sampling volume V_S was inferred from the PSR according to equation 1 as explained above. The obtained curve can actually be divided into two regions. Up to 15 mJ, the sampling volume is seen to grow larger with increasing energy with a steep slope. Contrariwise, only a very slight expansion is to be observed from 15 up to 60 mJ with a much lower slope. Eventually, the particle sampling volume does not prove to linearly expand from 3 to 60 mJ, almost saturating for a laser energy of around 15-20 mJ.

When analyzing silicon targets under similar experimental conditions by LIBS, namely using laser pulses of 5 ns duration at 532 nm, Milan and Laserna [21] observed a curve of similar shape plotting the evolution of the Si line at 288.158 nm as a function of laser fluence. The LIBS signal was found to saturate reaching a certain fluence value. Plasma shielding was concluded to explain such signal saturation. The same is very likely to apply when interrogating the liquid jet. There exists a laser fluence beyond which the sampling volume does not grow anymore owing to plasma shielding, preventing all of the laser pulse to reach the liquid jet.

The above presented results show how the sampling volume evolves with laser energy. Still, both the sampling volume and the SNR are expected to vary not only as a function of the deposited energy, but also through the laser fluence considering the interaction surface between laser pulses and the liquid jet. A first evaluation of this interaction surface can be made estimating the surface of the laser beam at $1/e^2$ of the peak intensity, assuming that the laser beam has an almost perfect Gaussian profile.

As no craters or marks may actually be printed on the liquid jet surface, the latter was replaced by a copper plate according to the following procedure. Images of the liquid jet were taken using the iCCD camera equipped with an objective and positioned perpendicularly to the laser beam. Position of the side-viewed surface of the liquid jet facing the laser beam was recorded identifying the corresponding vertical pixel row. The liquid jet was then replaced by a copper plate. Its side-viewed surface exposed to the laser beam was positioned

aligning it with the same vertical pixel row as that used to spot the exposed face of the liquid jet. Craters were then drilled in copper for laser energies identical to those used when probing the liquid jet. Crater diameter (considering the inner rim of the crater on the material surface) evolution as a function of laser energy is shown on figure 7. The experimental points were found to fit quite well with a logarithmic equation below writing:

$$Y = 3247 \ln X + 2389 \quad \text{Equation 2}$$

Assuming that the laser beam used in this study has a perfect round Gaussian shape, the theoretical formula of the surface of the beam section derived from that of the laser fluence writes:

$$S = \frac{S_0}{2} \ln\left[\frac{2E_{Laser}}{\pi \omega_0^2} \times \frac{1}{\Phi_{th}}\right] \quad \text{Equation 3}$$

where S is the crater surface of a particular point in the beam and S_0 is the surface at $1/e^2$. E_{Laser} is the maximum energy at the center of the beam, ω_0 represents the $1/e^2$ radius and ϕ_{th} the melting threshold fluence.

Identifying equation 2 with equation 3 allows determining S_0 whose value was found of about 6500 µm^2 corresponding to a diameter of around 90 µm. The applied laser fluence value was therefore estimated of around 235 J cm^{-2} with a laser energy of 15 mJ corresponding to saturation onset on figure 6.

4.4 Estimation of the sampled depth

The estimated value of the sampling volume was found to tend to saturate for energies of around 15-20 mJ with an estimated laser-jet interaction surface of about 90 µm. Though it may be difficult to determine a precise value of the sampling depth, it may be envisaged to assess its order of magnitude when probing a liquid jet in the conditions described above with nanosecond laser pulses of wavelength at 532 nm. At least two assumptions must be made to make an approximate calculation. First, the geometry of the sampling volume is not known with accuracy and must therefore be approximated by a cylinder. Second, the surface of the base of the cylinder may be approximated by S_0 assuming that the interaction surface between the laser pulses and the liquid jet is close to that value. Eventually, an estimation of the sampled depth h of around 7-10 µm may be drawn from the above calculated values of V_s (when saturation occurs, see figure 6) and S_0. It proves to be much lower than the liquid jet thickness L (≈ 1 mm) as $h / L << 1$. This indicates that an in-depth sampling is not achieved under such experimental conditions.

Considering estimations of thermal and optical penetration length compared with the above sampling depth tends to substantiate the hypothesis of plasma shielding. Indeed, depending on the material nature, the area affected by the laser pulses may be dominated either by thermal or optical processes [22]. The thermal penetration length may be inferred from the following expression:

$$L_{th} = \sqrt{\chi\,\tau}$$ Equation 4

where χ represents the thermal diffusivity and τ the laser pulse duration. Given that the laser pulse duration is of around 4 ns and considering the thermal diffusivity of pure water $\chi \approx 1.4 \times 10^{-7}$ m^2 s^{-1} [23], a rough estimation of the thermal penetration length was found of around a few tens of nanometers ($L_{th} \approx 25$ nm). The optical penetration length is contrariwise much higher than the thermal depth given that water is transparent to the laser wavelength at 532 nm (absorption coefficient $\gamma \approx 3.5 \times 10^{-4}$ cm^{-1} [24] and therefore L_{opt} >> 1mm). The liquid jet heating is therefore far more dependent on optical properties than on thermal features. Accordingly, volumic heating prevails over surfacic heating given that $L_{opt} >> L_{th}$. Still, the sampled penetration length verifies the following inequality when compared with its thermal and optical counterpart:

$$L_{th} < h < L_{opt}$$ Equation 5

This tends to support the hypothesis that the laser pulses can no longer pass through the liquid jet, being blocked by the nascent plasma growing in the liquid.

4.5 Comparison of the sampling volume with possible maximum sampling volume

Comparing the measured sampling volume with say, the volume corresponding to the intersection of the laser beam with the liquid jet can help getting a better insight of the efficiency of laser sampling. The latter volume delimitates the largest amount of liquid possibly sampled by the laser (assuming that water sampling is only mostly achieved through laser interaction and not assisted by plasma vaporization). This maximum sampled volume may be approximated multiplying the liquid jet thickness ($L \approx 1$ mm) by the roughly estimated laser-jet interaction surface S_0 (6500 µm^2). The so calculated volume MV_S (possible maximum sampling volume) equaling 10^{-6} cm^3 proves to be much larger than the sampling volume V_S which tends to saturate beyond 15-20 mJ with values of around 6 10^{-8} cm^3 ($V_S / MV_S << 1$). Thus, the estimations of the sampling volume V_S and depth h and their comparison with a possible maximum sampling volume MV_S and the liquid jet thickness L respectively make it clear that the area sampled by the laser remains confined near the liquid jet surface. Such

limitation has important consequences for the analysis of particles using a liquid jet in terms of sampling rate. Assuming a homogeneous distribution of particles within the liquid jet volume of cylindrical revolution, these results suggest that a large part of the particles will not be analyzed. Indeed, most of those located beyond the estimated sampling depth are not to be taken into account, thereby limiting the sampling rate using such configuration.

4.6 LIBS signal evolution as a function of particle sizes

When tackling the issue of the evolution of the LIBS signal-to-noise ratio as a function of various experimental parameters, the dependence of signal response as a function of particle sizes was broached first. Four suspensions with the same number concentration of 1.47 x 10^6 particles / cm^3 containing particles with monodisperse distributions of 2, 5, 8 and 10 µm were prepared. These were probed by LIBS recording series of individual spectra of 1000 laser shots with energy of 15 mJ. Positive spectra or particle hits were identified following the above described procedure (section 4.2). The same total number of spectra was selected among the positive spectra for each probed suspensions, and therefore each particle size. Four final spectra were obtained by ensemble averaging an equal number of particle hits. The dependence of peak to base ratio as a function of particle volume is presented on figure 8. The obtained graph shows that the LIBS signal does not vary as a function of particle size. As the LIBS signal is known to be proportional to the ablated mass, a linear dependence would be expected when carrying out these experiments. Two possible explanations may be suggested. Either such effect is the consequence of self-absorption or of non-complete vaporization of the particles, like that observed by Carranza and Hahn [25] when analyzing particles in air using LIBS. A similar result has recently been found by Diaz Rosado et al. [12] when analyzing micrometric-sized alumina particles in liquids using LIBS. A careful examination of the recorded data showed that non complete vaporization was very likely to be the cause of signal saturation. The graph of figure 8 shows likewise that borosilicate particles were not entirely vaporized either for sizes ranging from 2 to 10 µm.

4.7 SNR evolution as a function of laser energy

As explained above, the estimation of the sampling volume is of primary importance to pinpoint the intrinsic limitations of the coupling of LIBS with the liquid jet as a sampling technique for particle analysis and therefore the detection limits inherent to such approach. Investigations on the SNR must be carried out along with those on the sampling volume in order to assess the LIBS response. The evolution of the SNR as a function

of laser energy (see figure 9) was extracted from the very spectra recorded when analyzing the sampling volume (section 4.2). As already stated when examining the graph of figure 6 the curve depicting the evolution of the SNR as a function of laser energy may be divided into two regions. The SNR linearly rises from 3 mJ up to 15-20 mJ. Such rise is likely to be accounted for by the expansion of the sampling volume as depicted on figure 6. All like the sampling volume, the SNR happens to saturate for energies beyond 15-20 mJ for the same reason than that mentioned when scrutinizing figure 6, namely plasma shielding.

4.8 Optimizing the sampling volume and the SNR through proper laser fluence settings

The optimization of the LIBS signal (under the experimental conditions described in this paper) implies that of the sampling volume along with that of the SNR. Both the SNR and the sampling volume were found to saturate beyond a laser energy of around 15-20 mJ corresponding to an estimated fluence of around 235 J/cm^2. This result shows that systematically applying high laser fluences is no use, as neither the sampling volume nor the SNR increase with increasing energy. Increasing energy will only enhance mechanical ablation (caused by the action - reaction principle, the expanding plasma pushing back the liquid jet) within the liquid jet thereby making the inevitable problem of splashing gaining in importance.

5. Conclusion & perspectives

LIBS is deemed as a possible tool for in-situ analysis of particles for applications such as wastewater monitoring. With the aim in view to evaluate its potentialities in this context, suspensions of monodisperse borosilicate glass particles with sizes of 2, 5, 8 and 10 µm were analyzed coupling a liquid jet and LIBS. Nanosecond laser pulses at 532 nm with energies ranging from 3 to 60 mJ were utilized. The Ca I line at 422.672 nm was selected for spectrum recordings, the latter element being one of the major components of borosilicate particles. Thenceforth, the evolution of the sampling volume and of the SNR as a function of the laser energy was investigated. The dependence of the LIBS signal with different particle diameters was examined as well.

The sampling volume (along with the SNR) has been assessed using a conditional analysis procedure close to that implemented by Asgill and Hahn [20] when dealing with the analysis of micrometric-sized particles in air. It was found to linearly rise with laser energy up to 15 mJ whereas it exhibited saturation beyond this value. Such behavior was attributed to plasma shielding. Assuming an interaction surface equaling that at $1/e^2$ of the laser peak intensity experimentally estimated drilling marks in a copper plate, an estimation of the sampled depth was made. Along with these, a maximum accessible volume for sampling delimitated by the interaction of

the laser beam with the liquid jet was calculated. The comparison of the sampled volume and depth with the maximum accessible volume and the liquid jet thickness respectively clearly showed the surfacic nature of the interaction of the laser pulses with the liquid jet. Not all of the liquid jet thickness happens to be probed by the laser beam, thereby suggesting that particles positioned beyond the sampling depth are not taken into account for the analysis. The SNR was demonstrated to display the same tendency as that depicted by the sampling volume with signal saturation beyond 15 mJ. Last but not least, the LIBS signal (peak to base ratio) was found constant as a function of particle diameter, suggesting possible non-complete vaporization of particles. The latter explanation was confirmed by Rozado et al. [12] in an article dedicated to size effects occurring when analyzing particles by LIBS with a liquid jet.

Eventually, all these results point out the precautions of use and limitations of the liquid jet applied to particle analysis with LIBS using nanosecond pulse duration lasers at 532 nm. Indeed, laser fluence is to be set with care given that both the sampling volume and the SNR were seen to saturate. Increasing the laser fluence would only lead to increase splashing without improving the LIBS signal, only favoring mechanical ablation over liquid vaporization. Moreover, quantitative analysis of micrometric-sized particles may be seriously limited by non-complete vaporization of particles. The conclusions drawn from these experiments suggest the use of a liquid sampling technique more adapted to the issue of micrometric-sized particle detection than the liquid jet.

Acknowledgements

This research was supported by the French ministry of ecology, sustainable development and energy. We would like to thank M. Patrice Delalain for his assistance when using SEM and LDS instruments.

References

[1] D. W. Hahn and N. Omenetto, Laser-Induced Breakdown Spectroscopy (LIBS), Part I: Review of Basic Diagnostics and Plasma-Particle Interactions: Still-Challenging Issues Within the Analytical Plasma Community, Appl. Spectrosc. 64 (2010) 335A-366A

[2] D. W. Hahn and N. Omenetto, Laser-Induced Breakdown Spectroscopy (LIBS), Part II: Review of Instrumental and Methodological Approaches to Material Analysis and Applications to Different Fields, Appl. Spectrosc. 66 (2012) 347-473

[3] Y. Ito, O. Ueki, S. Nakamura, Determination of colloïdal iron in water by laser-induced breakdown spectroscopy, Anal. Chim. Acta 299 (1995) 401-405

[4] R. Knopp, F.J. Scherbaum, J.I. Kim, Laser-Induced Breakdown Spectroscopy (LIBS) as an analytical tool for the detection of metal ions in aqueous solutions, Fresenius J. Anal. Chem. 355 (1996) 16-20

[5] S. Nakamura, Y. Ito, K. Sone, Determination of an iron suspension in water by Laser-Induced Breakdown Spectroscopy with two sequential laser pulses, Anal. Chem. 68 (1996) 2981-2986

[6] C. Haisch, J. Lierman, U. Panne, R. Niessner, Characterization of colloïdal particles by Laser-Induced Plasma spectroscopy (LIPS), Anal. Chim. Acta 346 (1997) 23-25

[7] T. Bundschuh, J. I. Yun, R. Knopp, Determination of size concentration and elemental composition of colloids with Laser-Induced Breakdown Detection/Spectroscopy (LIBD/S), Fresenius J. Anal. Chem. 371 (2001) 1063-1069

[8] J.I. Yun, T. Bundschuh, V. Neck, J. I. Kim, Selective determination of Europium (III) oxide and hydroxide colloids in aqueous solution by Laser-Induced Breakdown Spectroscopy, Appl. Spectrosc. 55 (2001) 273-278

[9] H, Hotokezaka, N. Aoyagi, Y. Kawahara, N. U. Yamaguchi, S. Nagasaki, K. Sasaki, S. Tanaka, Selective and in-situ determination of carbonate and oxide particles in aqueous solution using Laser-Induced Breakdown Spectroscopy (LIBS) for wearable information equipment, Microsyst. Technol. 11 (2005) 974-979

[10] N. Yamaguchi, H. Hotokezaka, S. Nagasaki, S. Tanaka, Direct quantitative analysis of particulate aluminum suspended in water using Laser-Induced Breakdown Spectroscopy, Soil Sci. Plant Nutr. 51 (2005) 911-916

[11] S. C. Snyder, W. G. Wickun, J. M. Mode, B. D. Gurney, F. G. Michels, The detection of palladium particles in proton exchange membrane fuel-cell water by Laser-Induced Breakdown Spectroscopy, Appl. Spectrosc. 65 (2011) 642-647

[12] J. C. D. Rosado, D. L'hermite, Y. Levi, Effect of particle size on laser-induced breakdown spectroscopy analysis of alumina suspension in liquids, Spectrochim. Acta Part B 74-75 (2012) 80-86

[13] D. W. Hahn, W. L. Flower, K. R. Hencken, Discrete particle detection and metal emissions monitoring using laser-induced breakdown spectroscopy, Appl. Spectrosc. 51 (1997) 1836-1844

[14] J. E. Carranza, D. W. Hahn, Sampling statistics and considerations for single-shot analysis using laser-induced breakdown spectroscopy, Spectrochim. Acta Part B. 57 (2002) 779-790

[15] J. E. Carranza, D. W. Hahn, Plasma volume considerations for analysis of gaseous and aerosol samples using laser-induced breakdown spectroscopy, J. Anal. At. Spectrom. 17 (2002) 1534-1539

[16] P. K. Diwakar, K. H. Loper, A.-M. Matiaske, D. W. Hahn, Laser-induced breakdown spectroscopy, for analysis of micro-and nanoparticles, J. Anal. At. Spectrom. 27 (2012) 1110-1119

[17] U. Panne, D. Hahn, in: A.W. Miziolek, V. Palleschi, I. Schechter (Eds.), Laser-Induced Breakdown Spectroscopy, Cambridge University Press, 2006, chapter 5

[18] B. T. Fisher, H. A. Johnson, S. G. Buckley, D. W. Hahn, Temporal gating for the optimization of laser-induced breakdown spectroscopy detection and analysis of toxic metals, Appl. Spectrosc. 55 (2001) 1312-1319

[19] T. Amodeo, C. Dutouquet, O. Le-Bihan, M. Attoui, E. Frejafon, On-line determination of nanometric and sub-micrometric particle physicochemical characteristics using spectral imaging-aided Laser-Induced Breakdown Spectroscopy coupled with a Scanning Mobility Particle Sizer, Spectrochim. Acta Part B 64 (2009) 1141-1152

[20] M. E. Asgill, D. W. Hahn, Particle size limits for quantitative aerosol analysis using Laser-Induced Breakdown Spectroscopy: Temporal considerations, Spectrochim. Acta Part B 64 (2009) 1153-1158

[21] M. Milan, J. J. Laserna, Diagnostics of silicon plasmas produced by visible nanosecond laser ablation, Spectrochim. Acta Part B 56 (2001) 275-288

[22] I. Vladoiu, M. Stafe, C. Negutu, I. M. Popescu, The dependence of the ablation rate of metals on nanosecond laser fluence and wavelength, J. Optoelectron. Adv. Mater. 10 (2008), 3177-3181

[23] D.W. James, The thermal diffusivity of ice and water between -40 and +60 °C, J. Mater. Sci. 3 (1968) 540-543

[24] W. M. Irvine and J.B. Pollack, Infrared optical properties of water and ice spheres, ICARUS 8 (1968) 324-360

[25] J. E. Carranza, D. W. Hahn, Assessment of the upper particle size limit for quantitative analysis of aerosols using Laser-Induced Breakdown Spectroscopy, Anal. Chem. 74 (2002) 5450-5454

[26] Lines on line. http://physics.nist.gov/PhysRefData/ASD/lines_form.html

Figure captions

Figure 1. LIBS experimental setup.

Figure 2. SEM image of 5 µm-sized borosilicate glass particles.

Figure 3. Size distributions of borosilicate glass particles with sizes of 2, 5, 8 and 10 µm obtained using Laser Diffraction Spectrometry (LDS).

Figure 4. Temporal evolution of the signal to noise ratio (SNR) corresponding to the Ca I line at 422.672 nm obtained when analyzing a $CaSO_4$ solution for several energies ranging from 3 to 60 mJ.

Figure 5. Distribution of the percentage of spectra as a function of signal intensity normalized to the highest peak obtained when analyzing a suspension of 5 µm-sized particles using an energy of 15 mJ and time delay and gate width of 3 and 5 µs respectively. The vertical line represents the cut-off value under which peaks are no longer taken into account in the PSR calculation.

Figure 6. Evolution of the sampling volume as a function of the laser energy recorded for three series of spectra of 1000 laser shots each.

Figure 7. Evolution of the diameters of craters drilled on copper as a function of laser energy. The curve has been fitted by a logarithmic expression to deduce the laser beam section at $1/e^2$ of the peak intensity.

Figure 8. Evolution of the peak to base (P/B) ratio of the Ca line at 422.672 nm as a function of the particle volume for particulates with sizes of 2, 5, 8 and 10 µm recorded obtained when using a laser energy of 15 mJ.

Figure 9. Evolution of the signal to noise ratio (SNR) as a function of laser energy obtained using the same set of data as that utilized for figure 6.

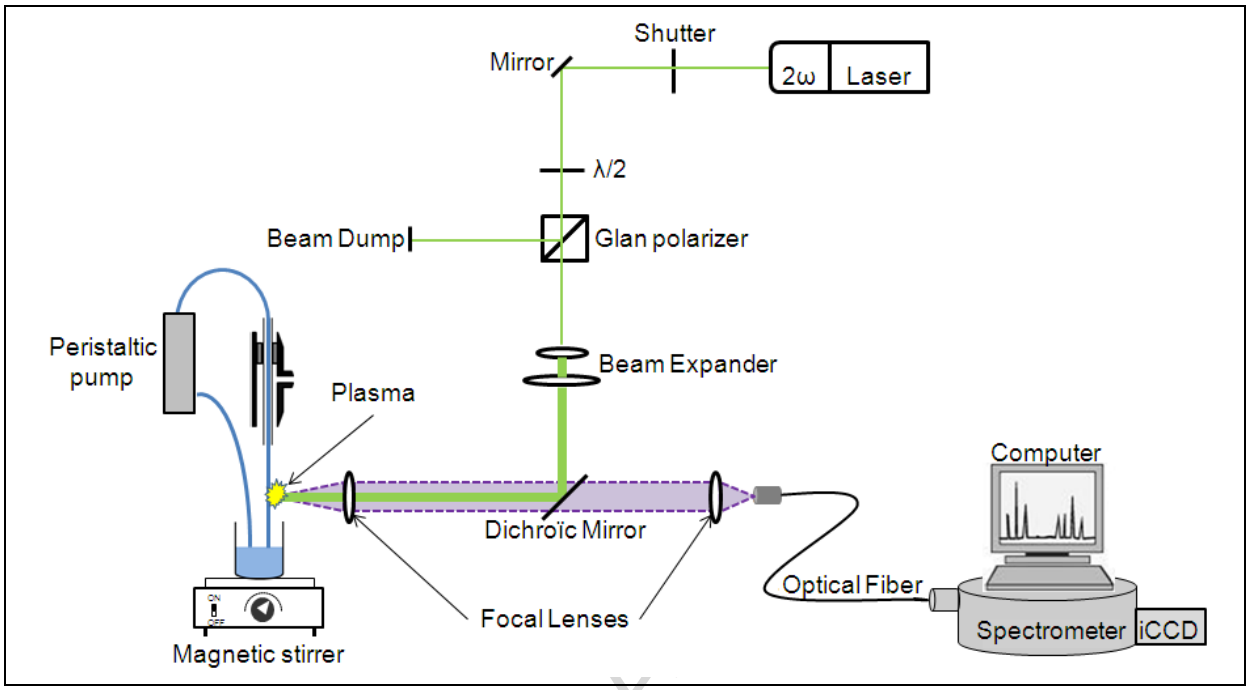

Figure 1

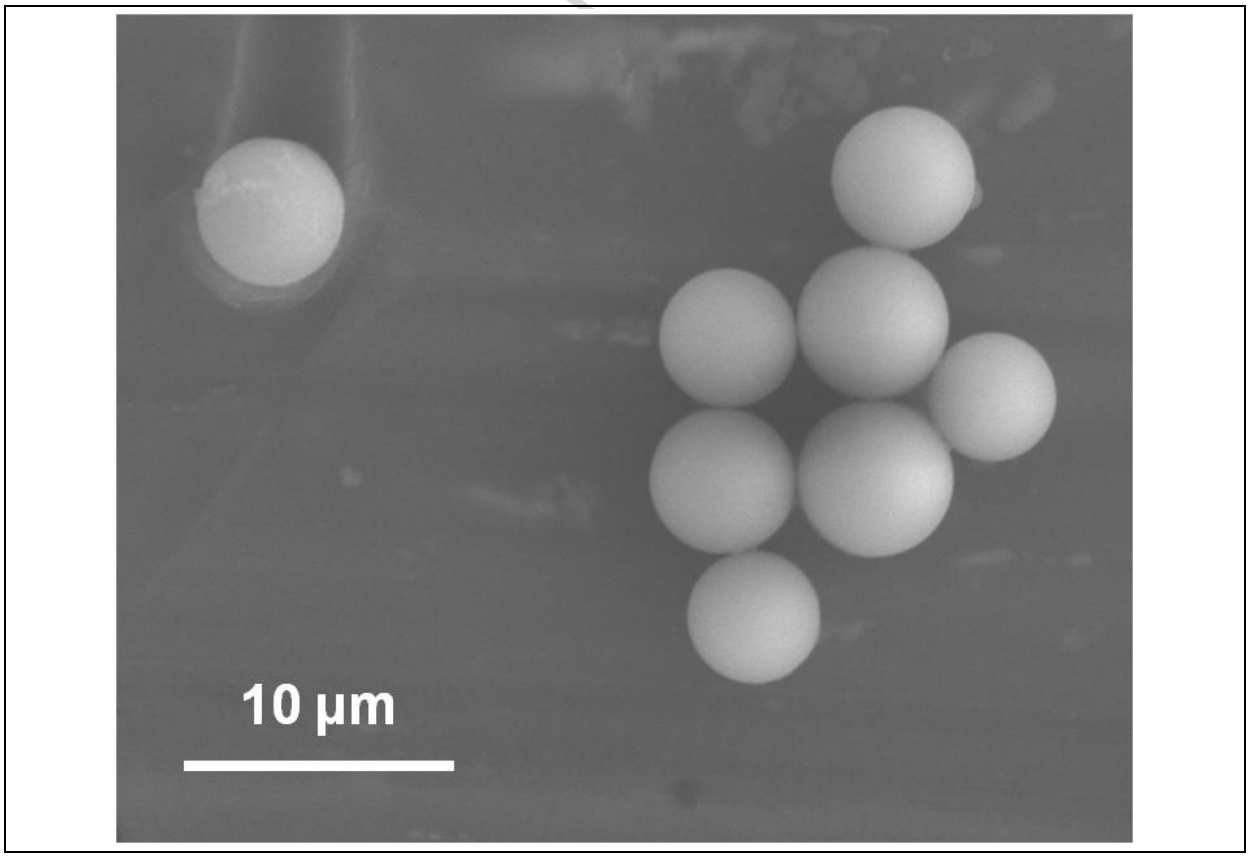

Figure 2

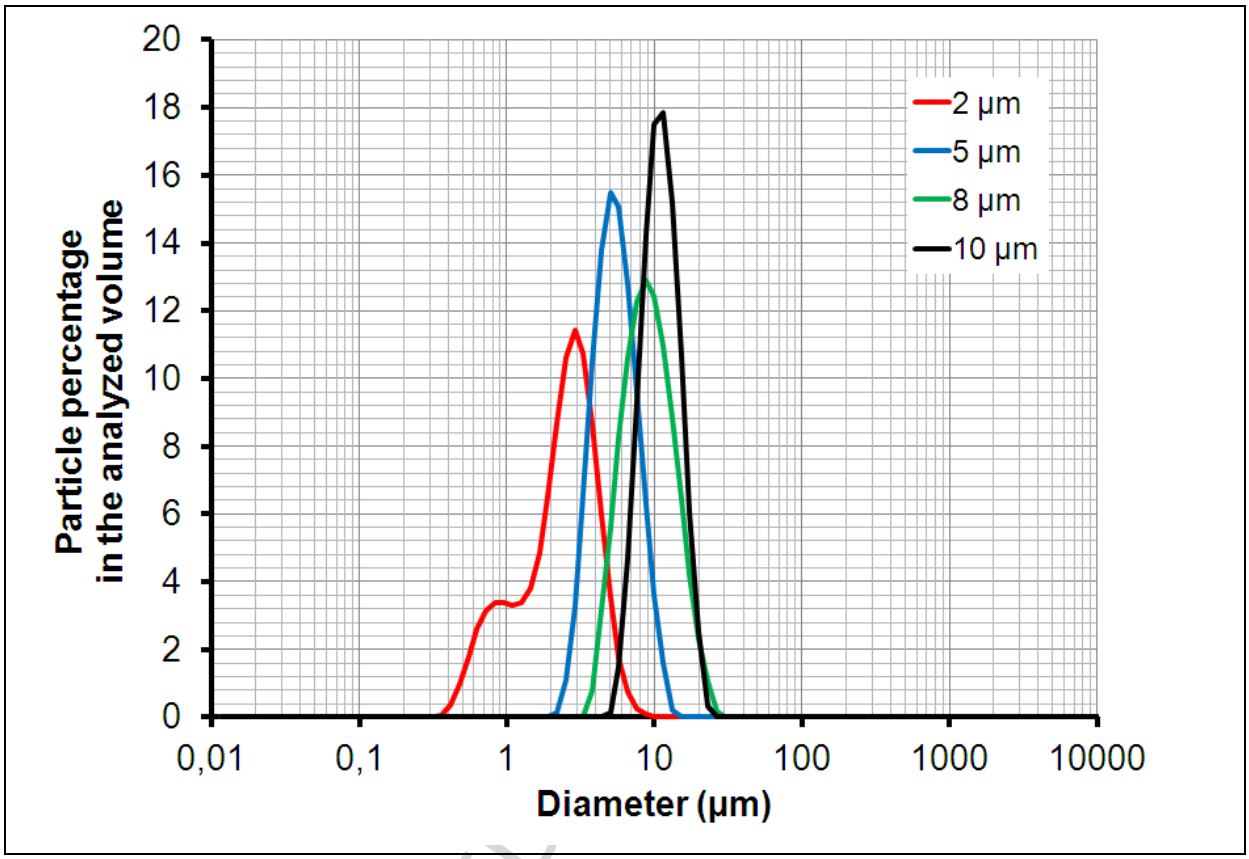

Figure 3

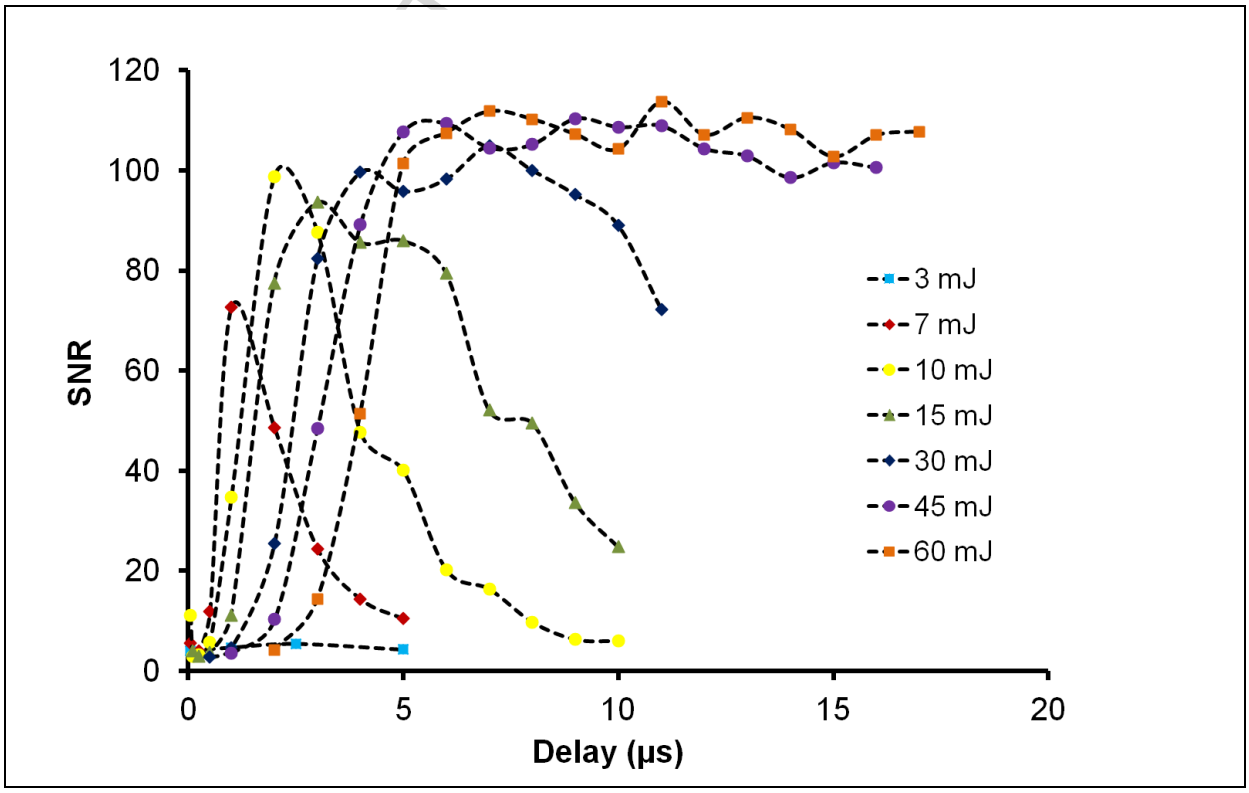

Figure 4

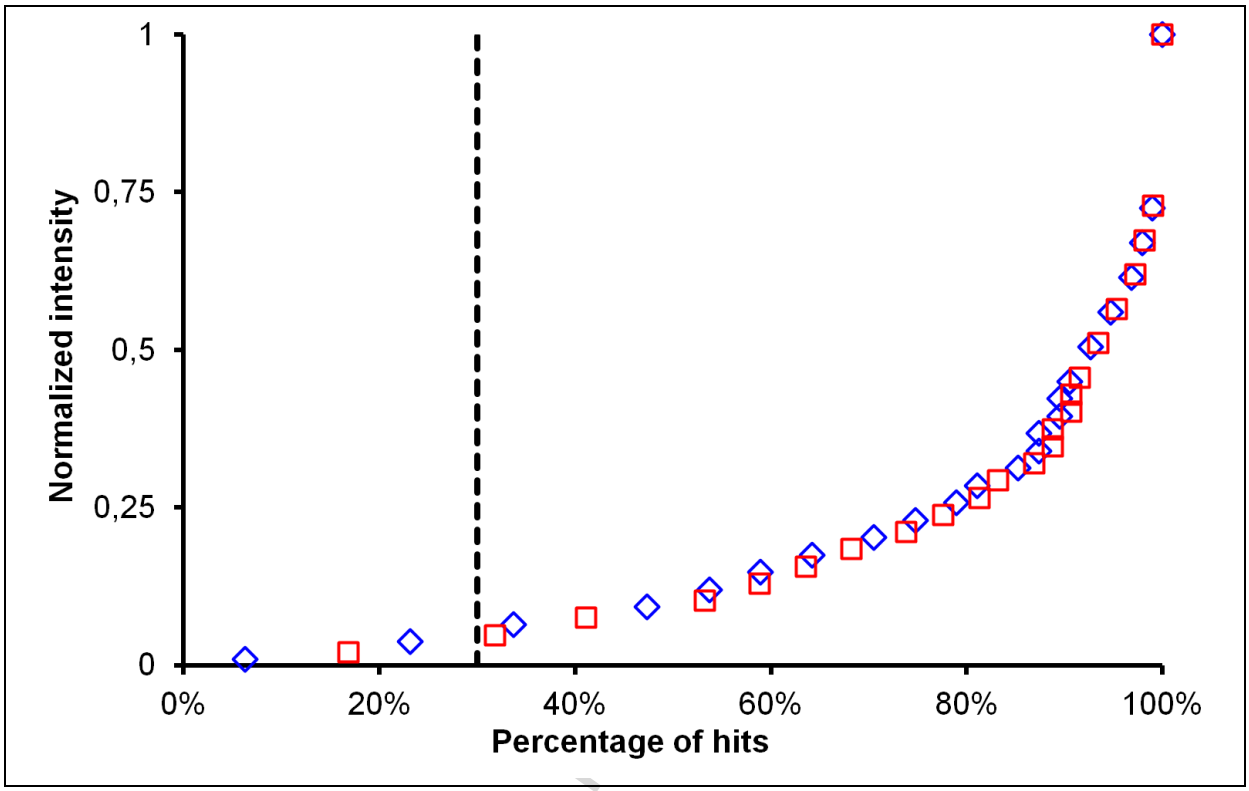

Figure 5

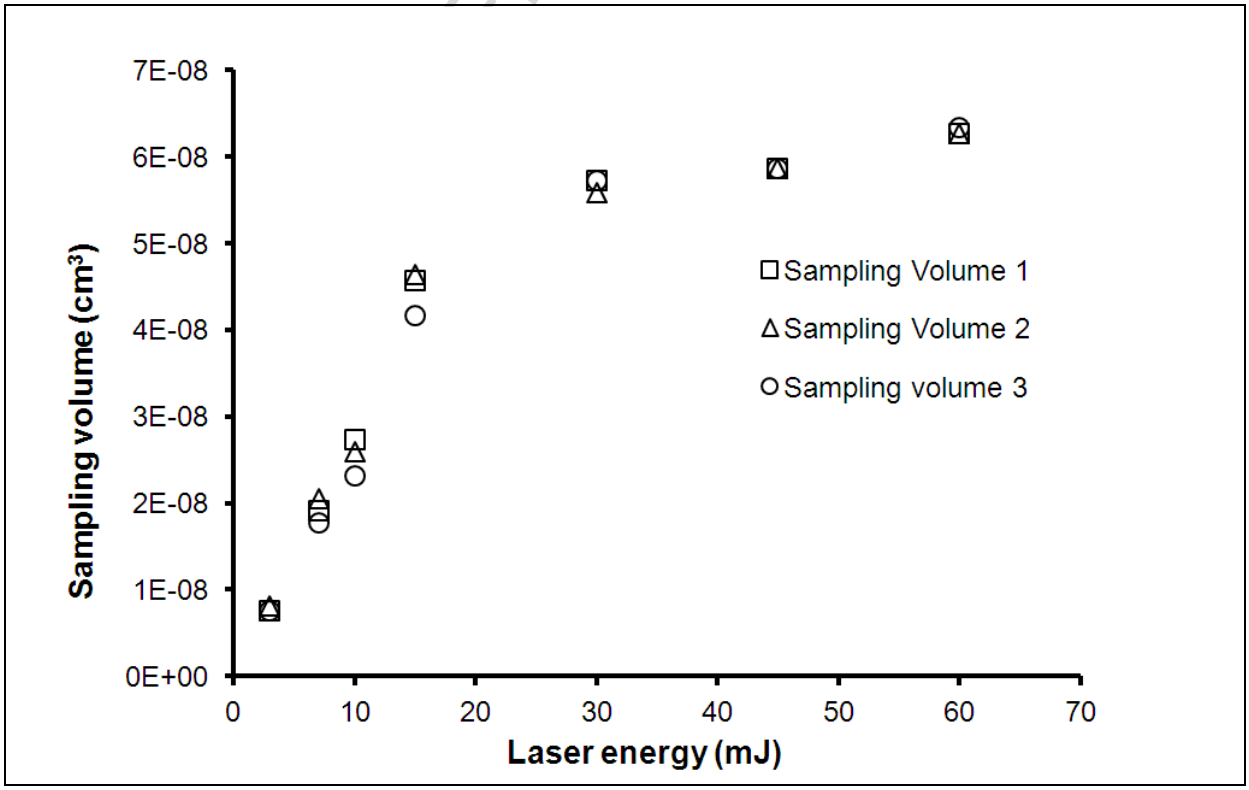

Figure 6

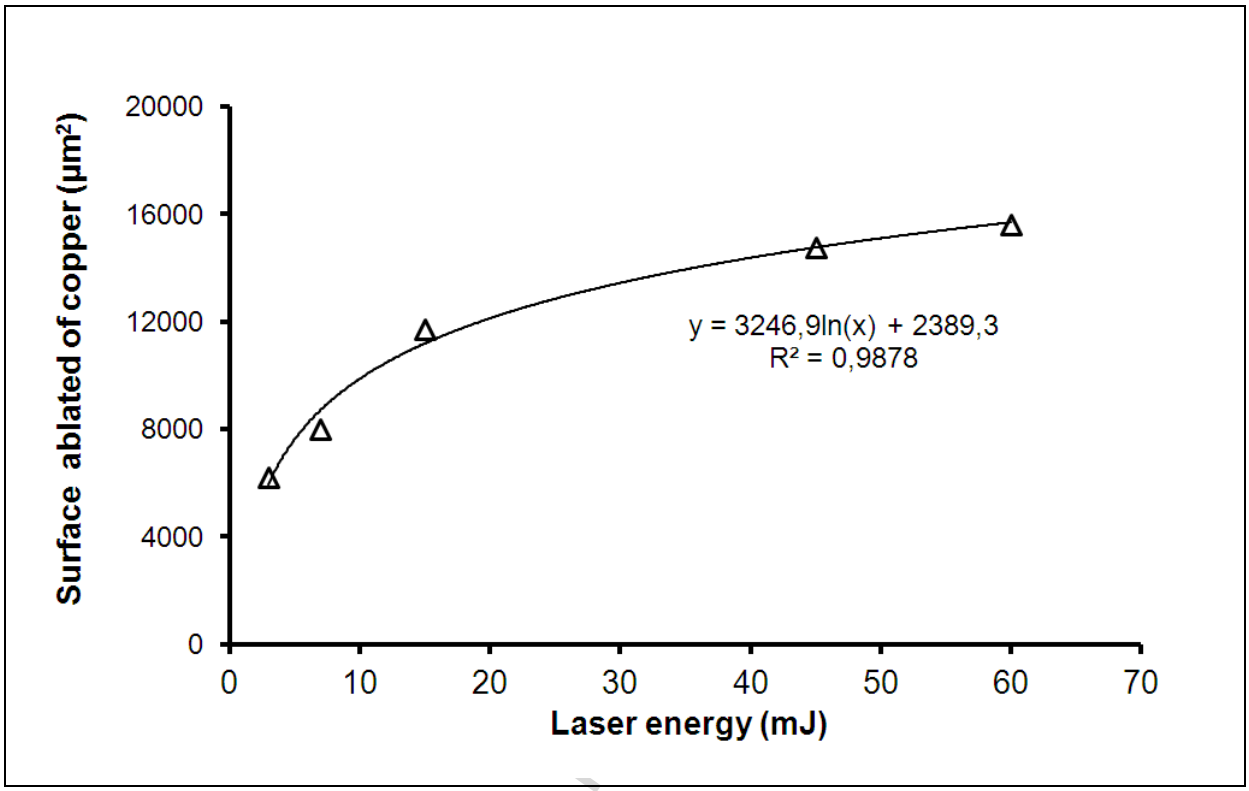

Figure 7

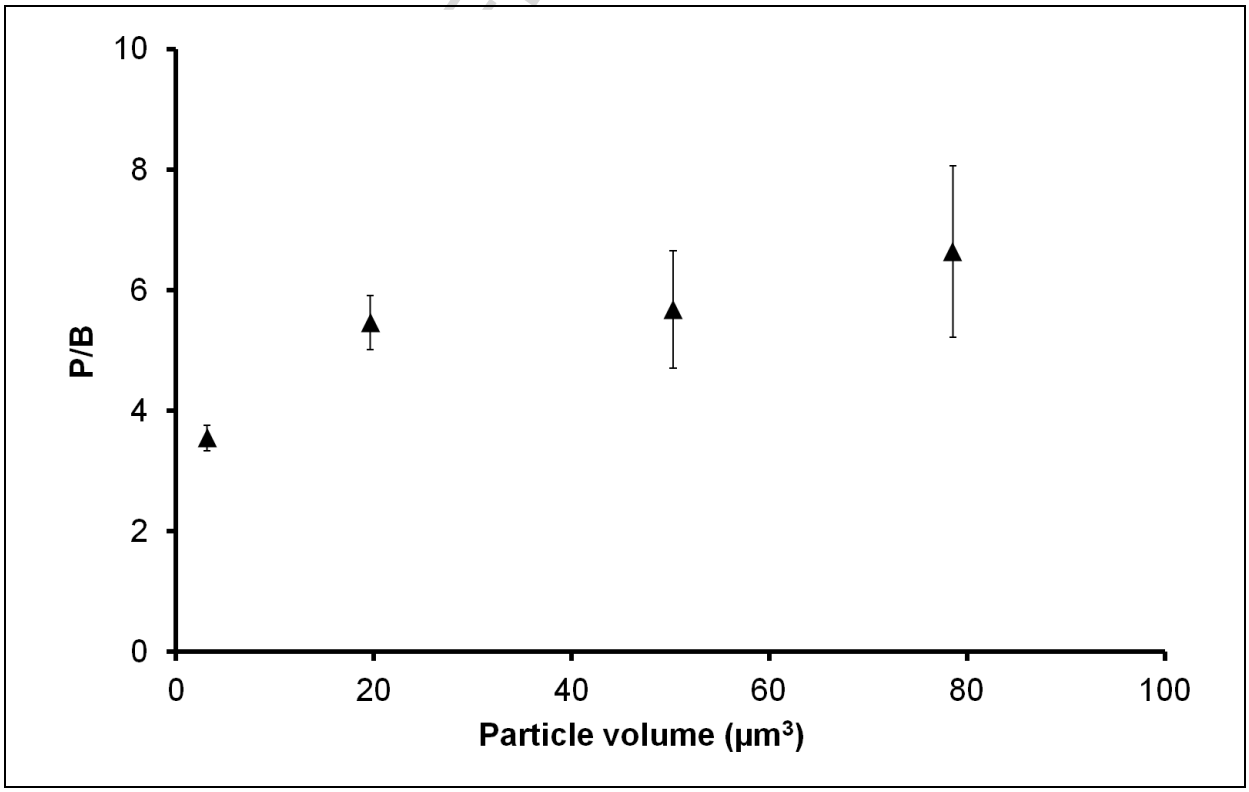

Figure 8

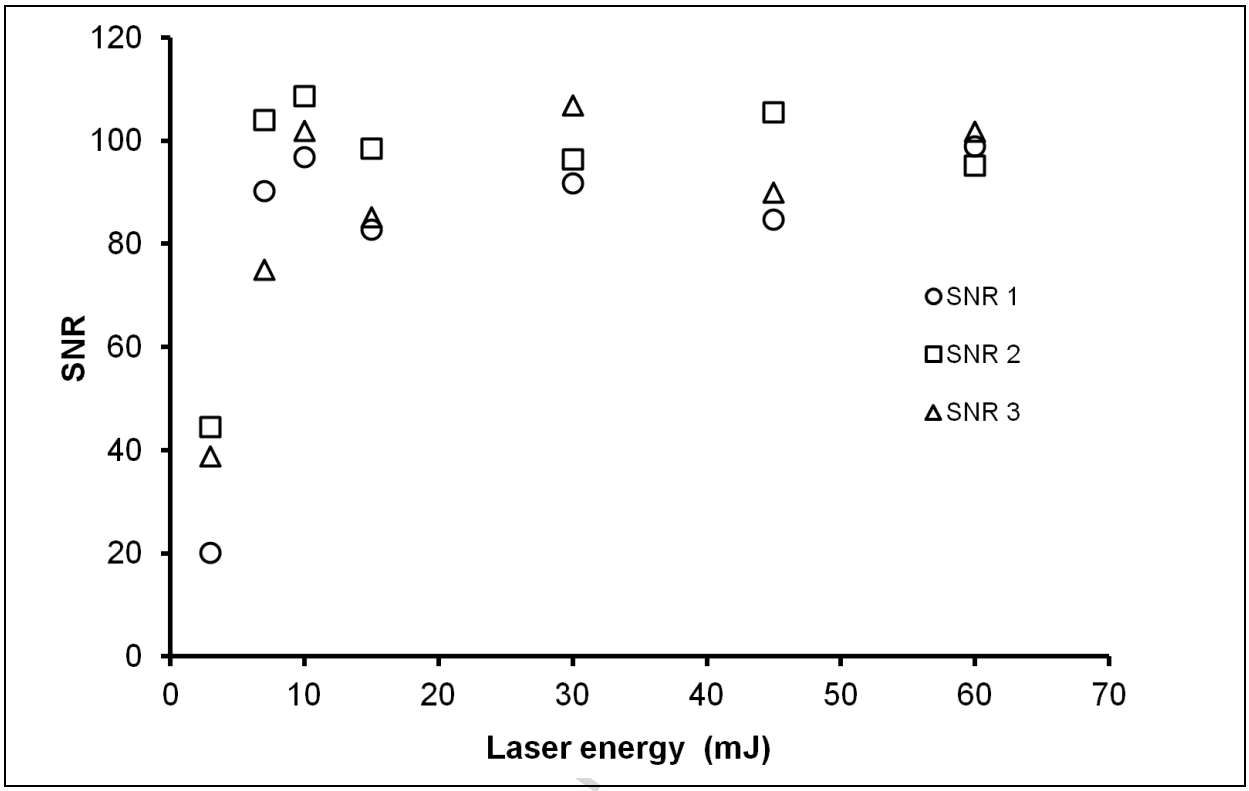

Figure 9

HIGHLIGHTS

- Micrometric-sized particles in suspensions are analyzed using LIBS and a liquid jet
- The evolution of the sampling volume is estimated as a function of laser energy
- The sampling volume happens to saturate beyond a certain laser fluence
- Its value was found much lower than the beam diameter times the jet thickness
- Particles proved not to be entirely vaporized
- Limitations of LIBS are thus evidenced when analyzing particles using a liquid jet